Am J Transl Res 2025;17(4):2467-2483
www.ajtr.org /ISSN:1943-8141/AJTR0163437

Original Article

Celastrol protects against diabetic nephropathy by modulating immune-related pathways: a bioinformatics and experimental validation

Xiaojuan Wang[1,2], Mohamad Hafizi Abu Bakar[1], Mohd Asyraf Kassim[1], Khairul Anuar Shariff[3], Libing An[2], Yan Qin[4]

[1]Bioprocess Technology Division, School of Industrial Technology, Universiti Sains Malaysia, Gelugor 11800, Penang, Malaysia; [2]Department of Pharmacy, Taishan Vocational College of Nursing, Tai'an 271099, Shandong, China; [3]School of Materials and Mineral Resources Engineering, Universiti Sains Malaysia, Nibong Tebal 14300, Penang, Malaysia; [4]Department of Rehabilitation, Taishan Vocational College of Nursing, Tai'an 271099, Shandong, China

Received January 20, 2025; Accepted March 19, 2025; Epub April 15, 2025; Published April 30, 2025

Abstract: Objectives: Celastrol has shown therapeutic effects in diabetic nephropathy (DN). This study aimed to elucidate its underlying mechanisms through bioinformatics analysis and experimental validation. Methods: Differentially expressed genes (DEGs) between DN and control groups were obtained from GSE30122 and GSE30528 datasets. Target genes of Celastrol were collected from relevant biological databases and intersected with the DEGs. Functional enrichment analysis was conducted to explore the associated biological processes. Immune cell infiltration in DN was analyzed, and a Lasso regression model was constructed to identify DN-associated gene markers with diagnostic potential. The binding affinity of celastrol to target proteins was evaluated using molecular docking. Additionally, high glucose (HG)-treated human kidney 2 (HK-2) cells were subjected to cell viability assays, flow cytometry, ELISA, and immunoblotting. Results: A total of 69 key target genes of celastrol were identified, primarily involved in oxidative stress, inflammation, and Phosphoinositide 3-Kinase (PI3K)/Protein Kinase B (Akt) signaling pathways. Immune cell infiltration analysis revealed significant differences in $CD4^+$ and $CD8^+$ T cell infiltration between the DN and control groups. Six key target genes were identified as strong diagnostic markers for DN, exhibiting high diagnostic accuracy. Molecular docking results revealed strong binding affinity between celastrol and three target proteins: Thrombospondin 2 (THBS2), membrane-associated guanylate kinase inverted 2 (MAGI2), and Fibroblast Growth Factor 9 (FGF9). *In vitro*, celastrol mitigated HG-induced damage in HK-2 cells, downregulating THBS2 expression while upregulating MAGI2 and FGF9 expression. Conclusion: Celastrol exerts protective effects on DN by modulating key molecular pathways, particularly those involved in inflammation and oxidative stress.

Keywords: Celastrol, diabetic nephropathy, network pharmacology, machine learning, molecular docking

Introduction

Diabetic nephropathy (DN) is one of the most prevalent and severe chronic microvascular complications of diabetes and a leading cause of end-stage renal disease (ESRD) [1, 2]. Emerging evidence suggests that proximal tubular injury plays a critical role in the pathogenesis of DN. The uptake of albumin by proximal tubules enhances the inflammatory response through cytokine and chemokine activation, ultimately promoting fibrosis [3]. Despite advances in medical management, the incidence and mortality rates associated with DN remain high. Epidemiological studies predict that by 2045, there will be 700 million diabetes patients worldwide, with approximately 40% expected to develop DN [4]. Currently, DN treatment primarily focuses on the strict glycemic and blood pressure control, along with the use of renin-angiotensin-aldosterone system (RAAS) inhibitors to slow disease progression [5, 6]. Metformin, sodium-glucose cotransporter 2 (SGLT2) inhibitors, and certain natural compounds such as polyphenols, flavonoids, and saponins have possible nephroprotective

https://doi.org/10.62347/CBIP6642

effects; however, further research is needed to fully elucidate their therapeutic potential [7, 8].

Celastrol, a bioactive compound derived from *Tripterygium wilfordii*, exhibits anti-inflammatory, anti-tumor, and neuroprotective properties [9-11]. It has been shown to inhibit reactive oxygen species (ROS) production, mitigate oxidative stress, and preserve mitochondrial function, thereby reducing inflammation [12]. Notably, celastrol's rapid absorption, extended half-life, and high bioavailability make it a promising candidate for therapeutic application [13]. Recent studies have explored its protective effects against the metabolic diseases, including insulin resistance, obesity, type 2 diabetes (T2D), and cardiovascular-related complications. Our previous research demonstrated that celastrol modulates cellular functions both *in vitro* and *in vivo*, particularly by attenuating mitochondrial dysfunction, reducing inflammation, and improving insulin resistance [14-19]. These properties make celastrol a promising candidate for the treatment of T2D [14]. Notably, celastrol has also demonstrated protective effects in DN. Study has shown that celastrol exerts its protective influence by upregulating sirtuin 1 (SIRT1), which inhibits the enhancer of zeste homolog 2 (EZH2)-mediated Wnt/β-catenin signaling pathway [15]. This pathway is implicated in fibrosis and inflammation, two major processes that contribute to the progression of DN. These findings highlight the therapeutic potential of celastrol in metabolic diseases, though the exact mechanisms remain to be elucidated.

Numerous studies have highlighted the critical role of genetic factors in the progression of DN. For instance, Tang et al. identified NTNG1 (netrin G1) and HGF (hepatocyte growth factor) as potential biomarkers for diabetic kidney disease through gene expression-based analysis [16]. Similarly, Xu et al. utilized the Gene Expression Omnibus (GEO) database, a publicly available collection of gene expression data, to identify 14 core genes associated with DN [17]. These genes are implicated in various biologic processes, such as inflammation, fibrosis, and oxidative stress, all of which are known contributors to the deterioration of kidney function in DN. These findings underscore the importance of genetic markers in the development and progression of DN, paving the way for further research into targeted therapies and diagnostics using bioinformatic approaches. With the advent of biological big data and advanced bioinformatics, researchers are now equipped to address the complexity of metabolic diseases more effectively. By integrating diverse data sources and leveraging computational tools, bioinformatics provides a holistic view of biological systems, enabling the identification of multiple molecular targets and pathways involved in disease progression [17, 18]. This broader, system-level approach is especially valuable for understanding the intricate mechanistic actions of celastrol, which are known to interact with several molecular networks simultaneously [12, 14, 16, 17, 19].

This study aims to elucidate the mechanisms by which celastrol exerts its therapeutic effects in DN and mitigates high glucose (HG)-induced damage in human kidney 2 (HK-2) cells. By analyzing multiple expression profile datasets from the Gene Expression Omnibus (GEO) database and comparing DN with control groups, we integrated *in silico* analyses with *in vitro* experiments to comprehensively investigate the protective mechanisms of celastrol. We utilized a bioinformatic approach to map the key gene interactions and pathways, followed by experimental validation to assess celastrol's effects on critical cellular processes, including fibrosis, inflammation, and oxidative stress. The combined *in silico* and *in vitro* strategy offers valuable insights into the multi-target effects of celastrol, enhancing our understanding of its role in diabetes-related complications. The brief flowchart of the study design is shown in **Figure 1**.

Methods

Data collection and preprocessing

DN-related datasets were obtained from the GEO database (https://www.ncbi.nlm.nih.gov/geo/). The datasets GSE30122 (containing 19 DN samples and 50 normal samples), GSE30528 (including 9 DN samples and 13 normal samples), and GSE30529 (including 10 DN samples and 12 normal samples) were downloaded for analysis. The idmap3 package in R4.2.2 (https://github.com/jmzeng1314/idmap3) was used to convert probe IDs of genes to gene names in these GEO datasets.

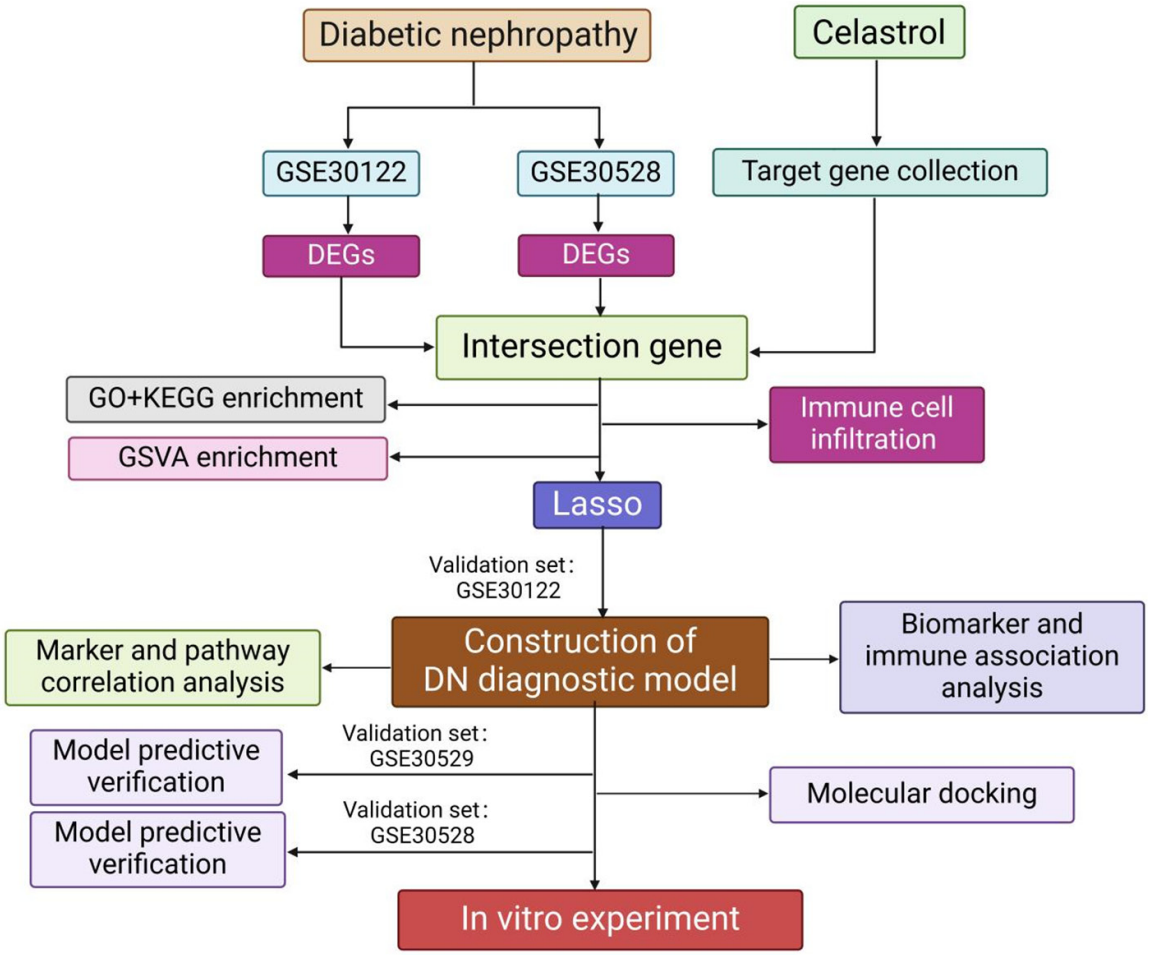

Figure 1. Graphical abstract. This study used GEO datasets (GSE30122, GSE30528, and GSE30529) to identify differentially expressed genes (DEGs) in diabetic nephropathy (DN). The target genes of celastrol were sourced from multiple databases and intersected with identified DEGs. The molecular docking was used to explore the binding affinity of celastrol to target proteins. Using cell-based assays, the human kidney 2 (HK-2) cells were treated with high glucose (HG) and celastrol, followed by cell viability (CCK-8), apoptosis (flow cytometry), and inflammation assays (ELISA). Immunoblotting was performed to assess the protein expression of fibrosis markers.

Collection of celastrol target genes

Target genes of celastrol were identified using the HIT2 (http://hit2.badd-cao.net/), CTD (https://ctdbase.org/), ETCM (http://www.tcmip.cn/ETCM/index.php/), and STITCH (http://stitch.embl.de/) databases with the keyword "Celastrol". Additionally, the SMILES structure of celastrol was obtained from the PubChem database. The potential target genes of celastrol were searched in Super-PRED (https://prediction.charite.de/), SwissTargetPrediction (http://swisstargetprediction.ch/), BATMAN-TCM (http://bionet.ncpsb.org.cn/batman-tcm/#/home), and PharmMapper (https://lilab-ecust.cn/pharmmapper/index.html) databases. After merging results and removing duplicates, a final list of celastrol target genes was established.

Identification of differentially expressed celastrol target genes

Differentially expressed genes (DEGs) between normal and DN samples were identified in the GSE30122 and GSE30528 datasets using the limma package in R4.2.2 (https://www.bioconductor.org/packages/release/bioc/html/limma.html). DEGs were defined using a p-value < 0.05 and |log2FC| > 0.1. The ggplot2 and pheatmap packages in R4.2.2 were used to create volcano plots and heatmaps of the

DEGs, respectively. Differentially expressed celastrol target genes were identified by intersecting the celastrol target genes with the DEGs. The VennDiagram package in R4.2.2 was used to visualize the intersection results.

Enrichment analysis of celastrol target genes

The clusterProfiler package in R4.2.2 was employed to conduct GO and KEGG pathway enrichment analyses on the differentially expressed target genes, with a significance threshold of $p < 0.05$. Results were visualized using ggplot2. Additionally, hallmark gene sets were downloaded from the MSigDB database (https://www.gsea-msigdb.org/gsea/msigdb). The Gene Set Variation Analysis (GSVA) package in R4.2.2 was used to compute enrichment scores for each sample in the GSE30122 dataset.

Immune cell infiltration analysis

The IOBR package in R4.2.2 was used to predict the immune cell infiltration levels in each sample from the GSE30122 dataset. The results were visualized using ggplot2. Differences in immune cell infiltration between DN and normal groups were analyzed using t-tests based on the CIBERSORT, TIMER, and xCell methods to identify key immune cell types.

Construction and validation of the DN diagnostic model

A classification model for DN diagnosis was constructed using the Lasso regression algorithm in the glmnet package in R4.2.2. The GSE30122 dataset served as the training set, while GSE30528 and GSE30529 were used as external validation sets. A 5-fold cross-validation was performed on the training set, with the lambda parameter set to lambda.1se.

Molecular docking analyses

Protein structures of the target molecules were downloaded from the RCSB Protein Data Bank (http://www.pdb.org/). The chemical structure of celastrol in "sdf" format was obtained from PubChem (https://pubchem.ncbi.nlm.nih.gov/) and converted to PDBQT format using the Open Babel GUI software. Protein preparation included ligand removal, dehydration, hydrogen addition, amino acid optimization, and charge calculation. Molecular docking was performed using Autodock1.5.7, and docking results were visualized with Pymol.

Cell culture and treatment

HK-2 cells, obtained from Shanghai Binsui Biotechnology Co., Ltd. (Shanghai, China), were cultured in Dulbecco's modified Eagle's medium (DMEM)/F12 (no. 11320033, Gibco, NY, USA) supplemented with 10% fetal bovine serum (FBS, no. 10270-106, Gibco, NY, USA) in a 5% CO_2 incubator maintained at 37°C. Cells in their logarithmic growth phase were seeded into 6-well plates at a density of 3×10^4 cells per well (100 µL). They were then allocated into the following groups: negative control (NC, exposed to normal glucose levels), high glucose (HG), and HG + cel (treated with high glucose and 20 nm, 50 nM, or 100 nM celastrol for 24 h). For the HG treatment, the growth medium was supplemented with 50 mmol/L glucose. Celastrol (Sigma) was dissolved in dimethyl sulfoxide (DMSO, no. 102510041, Sigma-Aldrich Corporation, Missouri, USA) and freshly diluted to the target concentration before use.

Cell viability assessment using CCK-8 assay

To assess the viability of HK-2 cells, the CCK-8 assay was conducted. HK-2 cells in the logarithmic growth phase were seeded into 96-well plates at a density of 4×10^3 cells per well, with three replicates for each experimental group. After 24 h incubation, 10 µL of CCK-8 reagent (no. F25, SciBioCold, Beijing, China) was added to each well and incubated for 1 h. Subsequently, the absorbance at 450 nm for each well was measured to determine cell viability.

Flow cytometry for cell apoptosis

Flow cytometry was employed to quantify cell apoptosis. HK-2 cells were seeded at a density of 1×10^6 cells/well in 6-well plates and cultured for 48 h under standard conditions. After treatment, the cells were digested using 0.25% trypsin (without EDTA), collected, and centrifuged at 1000 rpm for 5 min. The supernatant was discarded, and the cell pellet was washed with 1 mL of pre-chilled (4°C) PBS. Cells were then resuspended in 1 mL of Annexin V binding buffer, adjusting the final cell concentration to 1×10^6 cells/mL. Subsequently, 100 µL of the

cell suspension was incubated with 5 μL of Annexin V-FITC (from the FXP018 Cell Apoptosis Detection Kit, Sichuan Baiao Biological Technology Co., Ltd.) at room temperature in the dark for 5 min. Then, 10 μL of propidium iodide (PI, 20 μg/mL) was added, followed by 400 μL of PBS. Apoptotic cells were analyzed immediately using a BeamCyte-1026 flow cytometer (Biotime Technology Co., Ltd.). Data were processed using FlowJo v10 software (TreeStar, USA).

Enzyme-Linked Immunosorbent Assay (ELISA)

To quantify the levels of the inflammatory markers, interleukin-6 (IL-6) and tumor necrosis factor-alpha (TNF-α), in HK-2 cells, an ELISA was conducted. HK-2 cells were cultured for 24 h, and the culture medium was collected and centrifuged at 1000×g for 5 min. The supernatant was transferred to an Eppendorf tube for analysis. Following the protocol provided with the ELISA kit (no. SEA079Hu, SEA133Hu, Wuhan USCN Business Co., Ltd., Wuhan, China), blank wells, standard wells, and sample wells were prepared. The ELISA solution was added to each well, and the optical density was measured at 450 nm using a microplate reader.

Western blotting

Protein was extracted from HK-2 cells on ice, and concentrations were determined using the BCA assay. Briefly, 30 μg of protein from each sample was loaded onto an SDS-PAGE gel. Following electrophoresis, the proteins were transferred onto PVDF membranes [14, 16]. The membranes were then blocked for 2 h and incubated overnight at 4°C with primary antibodies specific to collagen IV (Col IV, no. AF0510, Affinity Biosciences, Shanghai, China), fibronectin (FN, no. AF5335, Affinity Biosciences, Shanghai, China), α-smooth muscle actin (α-SMA, no. AF1032, Affinity Biosciences, Shanghai, China), thrombospondin 2 (THBS2, no. DF14754, Affinity Biosciences, Shanghai, China), membrane-associated guanylate kinase inverted 2 (MAGI2, no. AF0492, Affinity Biosciences, Shanghai, China), and fibroblast growth factor 9 (FGF9, no. DF9532, Affinity Biosciences, Shanghai, China). Then, the membranes were incubated with a secondary IgG antibody (no. GB23303, Servicebio Technology Co., Ltd., Wuhan, China) at room temperature for 2 h. Protein bands were visualized using an enhanced chemiluminescence reagent (no. M2301, HaiGene, Heilongjiang, China) and captured with a gel imaging system. Band intensity was analyzed using ImageJ software.

Statistical analysis

Statistical analyses were performed using GraphPad Prism 10.1.2 software. Data were expressed as mean ± standard deviation. Multi-group comparisons were performed using one-way analysis of variance (ANOVA), followed by Tukey's test for pairwise comparisons. Statistical significance was set at $P < 0.05$.

Results

Identification of DEGs in DN and key targets of celastrol

As shown in **Figure 2A**, **2B**, a total of 3416 and 1710 DEGs were identified in the GSE30122 and GSE30528 datasets, respectively. The top 100 DEGs from each dataset were visualized using heatmaps. Additionally, 750 celastrol target genes were retrieved. By intersecting the DEGs with celastrol target genes, 69 overlapping genes were identified and designated as the key celastrol target genes (**Figure 2C**). The interactions between celastrol and key target genes are depicted in **Figure 2D**.

Functional analysis of celastrol's key targets in response to oxidative and inflammatory stimuli

Functional analyses were performed on the key targets, identifying 1447 GO terms (including 1261 biological processes [BPs], 69 cellular components [CCs], and 117 molecular functions [MFs]) and 14 KEGG pathways. As depicted in **Figure 3A**, **3B**, the top five BPs were cellular response to oxidative stress, regulation of inflammatory response, positive regulation of cell activation, response to oxidative stress, and cellular response to chemical stress. CCs were mainly related to focal adhesion, external side of plasma membrane, collagen-containing extracellular matrix (ECM), membrane microdomain, and membrane raft. MFs were predominantly associated with glycosaminoglycan binding, phosphatase binding, protein tyrosine kinase activity, growth factor binding, and amide binding. Additionally, the top five KEGG

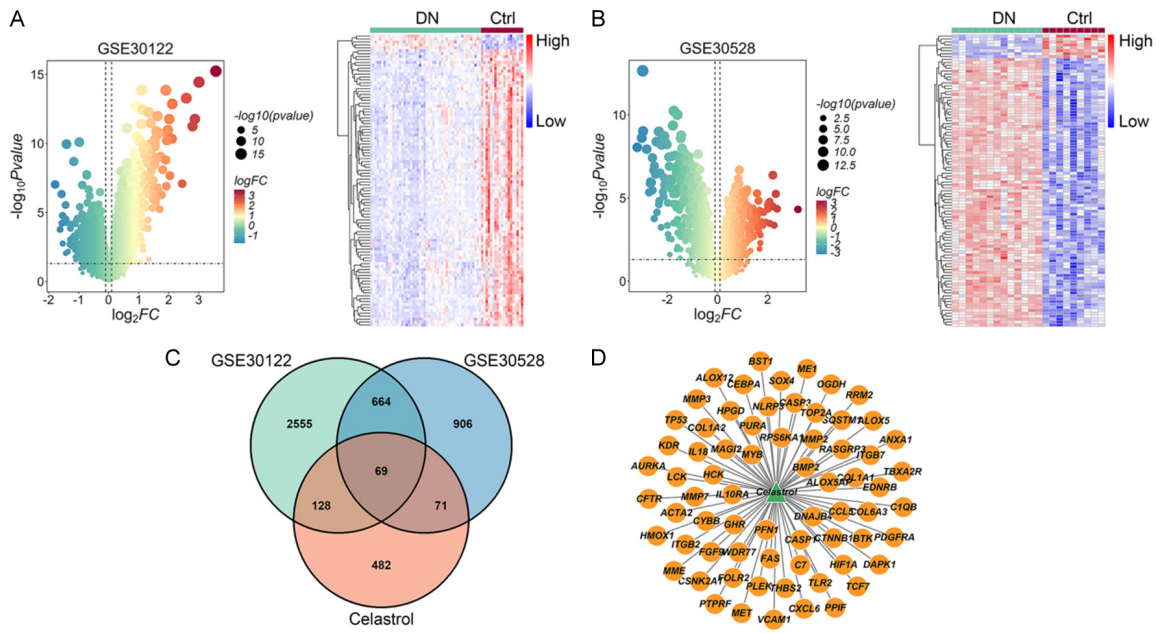

Figure 2. Identification of DEGs in DN and key targets of celastrol. A. Volcano plot of DEGs and heatmap of top 100 DEGs in GSE30122. B. Volcano plot of DEGs and heatmap of top 100 DEGs in GSE30528. C. Venn diagram between DEGs and celastrol targets. D. The relationship between celastrol and 69 key gene targets. Notes: DEG, differentially expressed genes; DN, diabetic nephropathy.

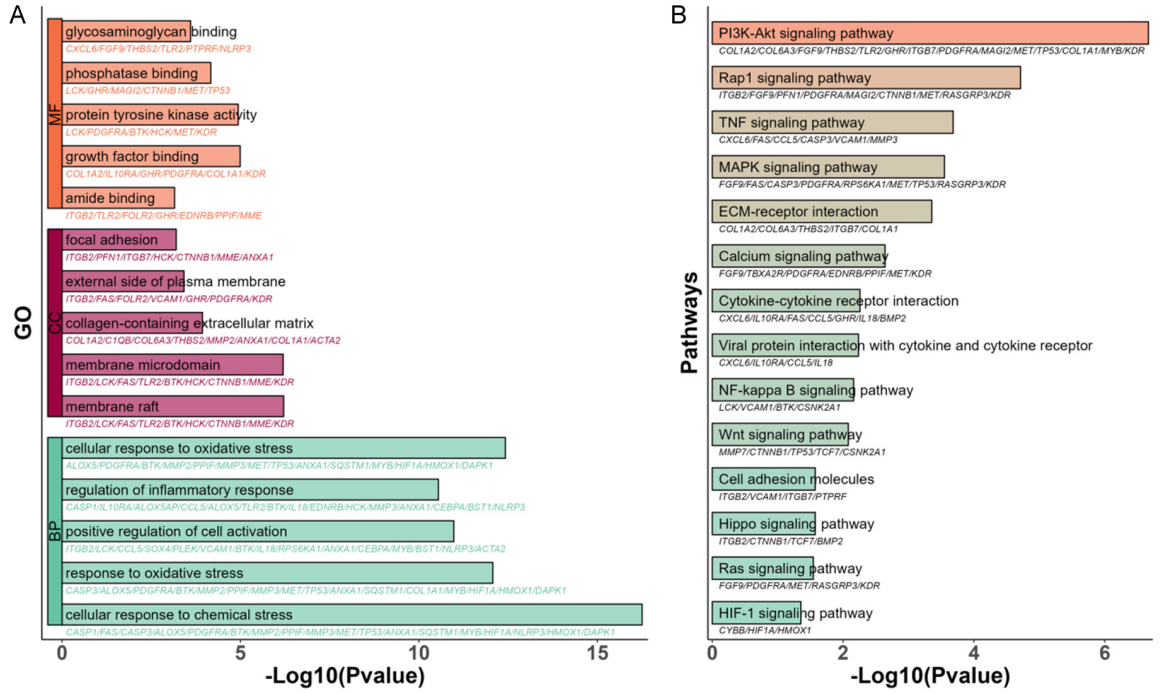

Figure 3. Functional enrichment analysis of key celastrol targets. A. Top 15 Gene Ontology terms, including 5 molecular functions, 5 cellular components, and 5 biological processes. B. Significant 14 Kyoto Encyclopedia of Genes and Genomes (KEGG) pathways.

pathways included PI3K/Akt signaling pathway, Rap1 signaling pathway, TNF signaling pathway, MAPK signaling pathway, and ECM-receptor interaction, with the PI3K/Akt signal-

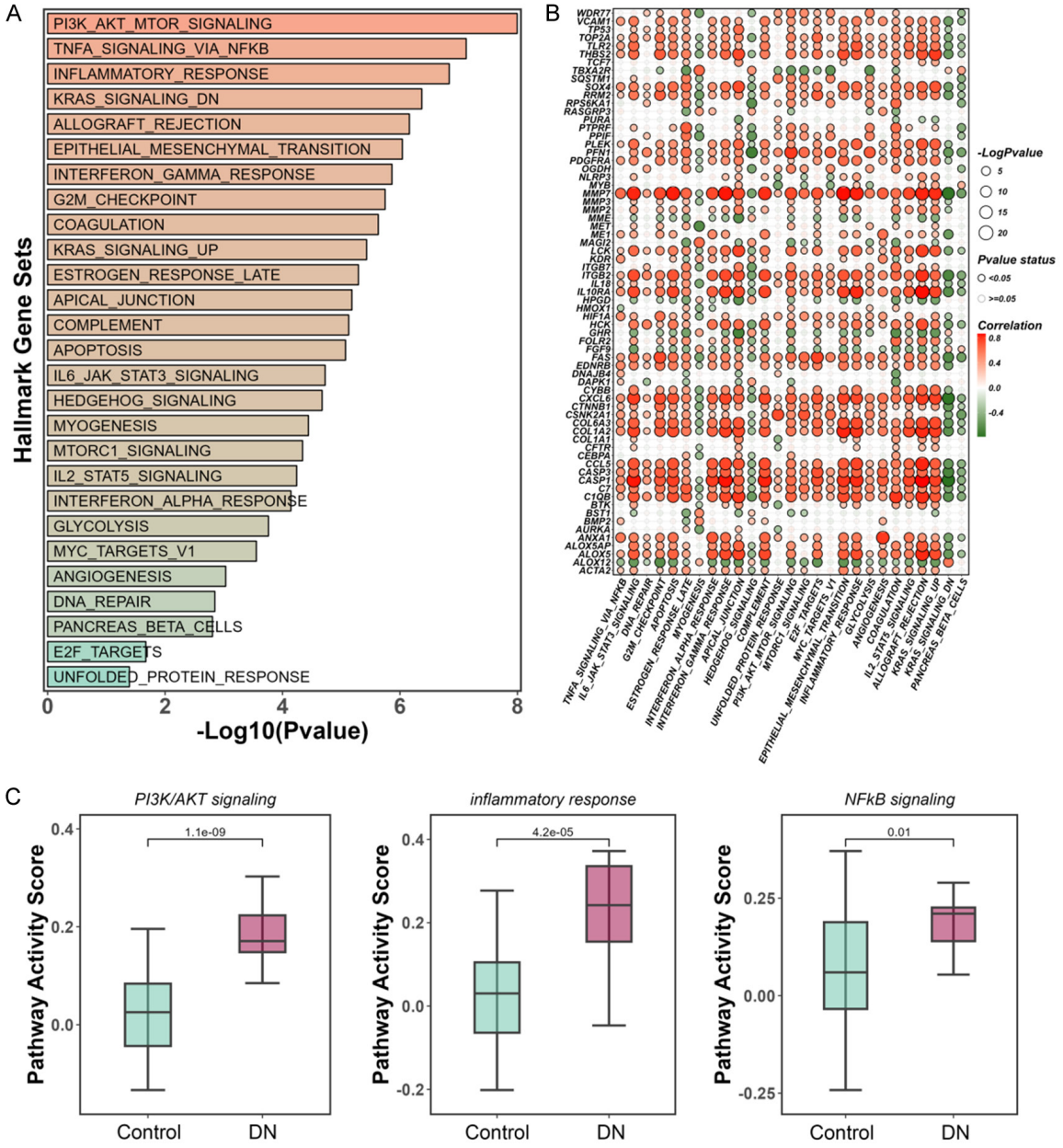

Figure 4. The pathway activity scores based on gene set variation analysis (GSVA). A. Bar plot of GSVA pathway activity scores; the redder the color of the bars, the more significant the *p* value. B. Heatmap of key target gene-GSVA pathway correlations. C. PI3K/AKT, NF-κB/TNF-α, and inflammatory pathways activity score.

ing pathway being the most significantly enriched (**Figure 3B**).

Prediction of celastrol's effect on PI3K/AKT, NF-κB/TNF-α, and inflammatory pathways

To further investigate the mechanisms by which celastrol influences the development of DN, pathway activity scores of hallmark gene sets were analyzed in the GSE30122 samples. A total of 27 pathways demonstrated significant differences in scores between the DN and control groups ($P < 0.05$). Among these, the PI3K/AKT, NF-κB/TNF-α, and inflammatory response pathways exhibited the most significant differences (**Figure 4A**). The scores of these three pathways were positively correlated with many key celastrol-targeted genes ($P < 0.05$, **Figure 4B**). Importantly, the scores of these three pathways were significantly higher in the DN

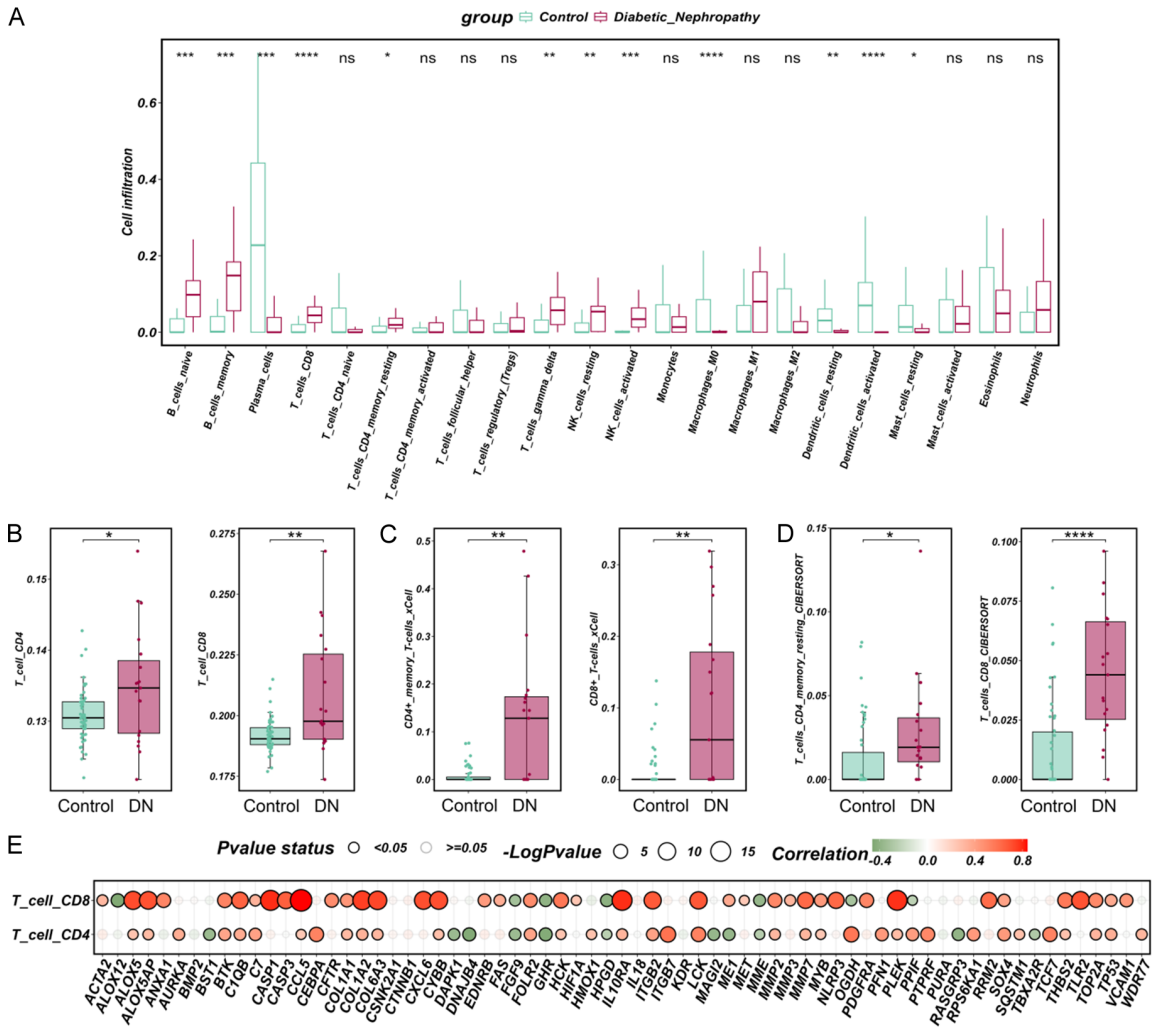

Figure 5. Immune cell infiltration analysis. (A) Immune cell infiltration analyzed using CIBERSORT; *P < 0.05, **P < 0.01, ***P < 0.001, ****P < 0.0001, ns: no significant. (B-D) Abundance of CD4 T cells and CD8 T cells analyzed using (B) CIBERSORT, (C) TIMER, and (D) xCell; *P < 0.05, **P < 0.01, ****P < 0.0001. (E) Correlation of CD4 T cells and CD8 T cells with key targets.

group compared to the control group (all P < 0.05, **Figure 4C**).

Immune infiltration analysis of differential CD4 and CD8 T cell abundance in DN

Given the enrichment of immune-related pathways identified in the preceding analyses, immune cell infiltration patterns were further examined. The CIBERSORT algorithm revealed significant differences in the abundance of most immune cells between DN and control groups (P < 0.05, **Figure 5A**). Subsequent analyses using the TIMER and xCell algorithms revealed that CD4 and CD8 T cell counts were consistently and significantly different between the two groups (P < 0.05, **Figure 5B-D**). In addition, T cell functional status scores, such as quiescence, senescence, terminal exhaustion, cytotoxicity, helper function, and regulatory activity, were significantly higher in DN samples compared to controls (Figure S1). These results suggest that T cells may play an important role in DN pathogenesis. Further correlation analysis revealed that CD4 and CD8 T cell abundances were positively associated with most key celastrol target genes (**Figure 5E**).

Development of a diagnostic model for DN based on lasso regression of key marker genes

Subsequently, a Lasso regression analysis was conducted on the 69 key target genes to con-

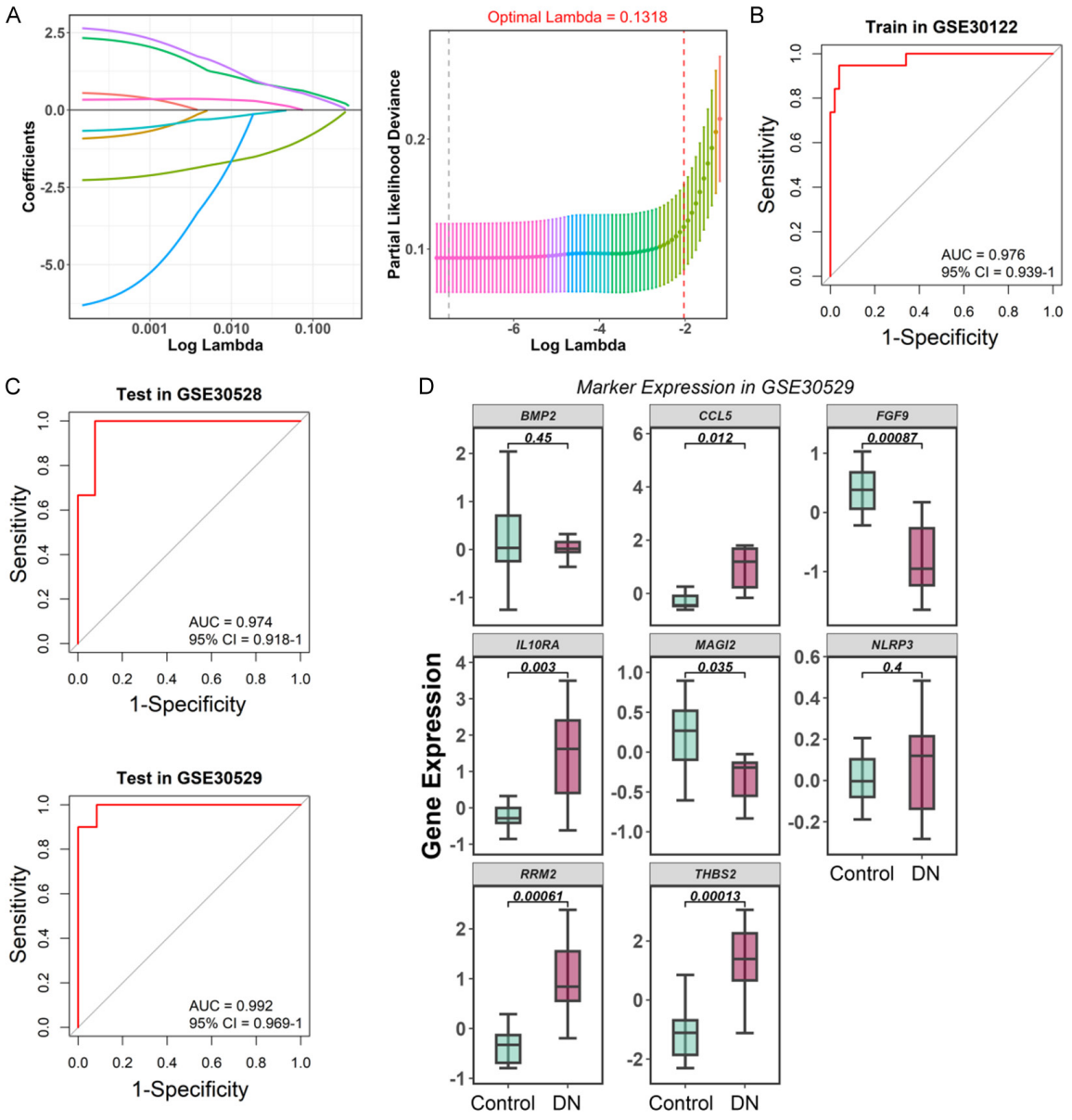

Figure 6. Construction and evaluation of diagnostic model to enhance the accuracy and interpretation of DN-associated gene markers. A. Lasso regression analysis. B. Evaluation of diagnostic model in GSE30122 dataset. C. Validation of diagnostic model in GSE30528 and GSE30529 datasets. D. Expression levels of marker genes in GSE30529 dataset. AUC: area under curve.

struct a diagnostic model for DN. At λ = 0.1318, the optimal classification diagnostic model was constructed, comprising 8 key target genes: THBS2, MAGI2, FGF9, nucleotide-binding domain, leucine-rich - containing family, pyrin domain - containing-3 (NLRP3), Interleukin-10 receptor subunit alpha (IL10RA), bone morphogenetic protein 2 (BMP2), ribonucleoside-diphosphate reductase subunit M2 (RRM2), and chemokine ligand 5 (CCL5) (**Figure 6A**). The model's performance was evaluated in the GSE30122 dataset, yielding an area under the receiver operating characteristic (ROC) curve (AUC) value of 0.976, indicating excellent diagnostic value (**Figure 6B**). To mitigate overfitting, external validation was performed using the GSE30528 and GSE30529 datasets, which demonstrated high AUC values of 0.974 and 0.992, respectively (**Figure 6C**).

Furthermore, the expression of the 8 key target genes was validated in the GSE30529 dataset.

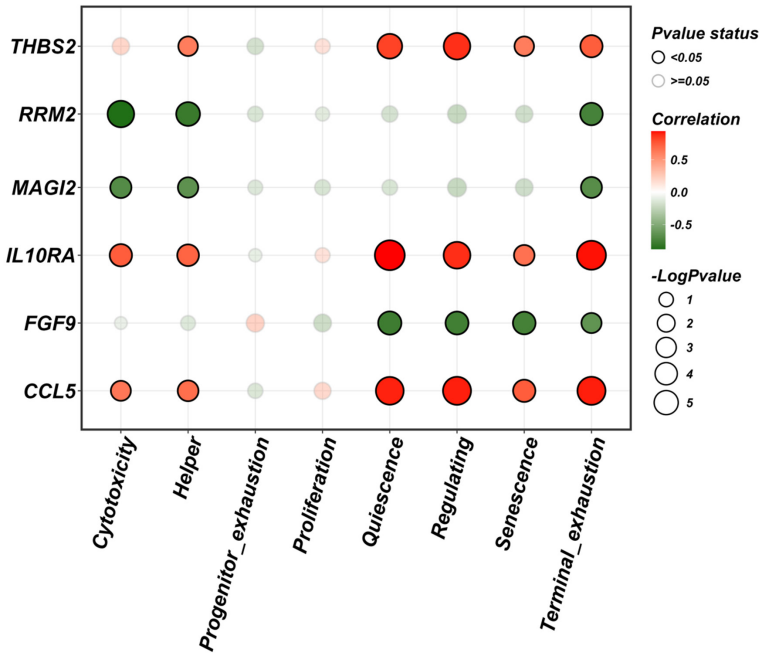

Figure 7. Correlation between six target genes and 8 T cell states.

Table 1. Molecular docking analysis between celastrol and the top 6 hub genes

Target	Uniprot	PDB	Pubchem_ID	Compound	Free binding energy (kcal/mol)
THBS2	P35442	1yo8	122724	Celastrol	-7.684
FGF9	P31371	1g82			-7.581
MAGI2	Q86UL8	1uep			-7.042
CCL5	P13501	5coy			-6.957
BMP2	P12643	6omn			-6.751
RRM2	P31350	3olj			-6.667

Except for BMP2 and NLRP3, the remaining 6 target genes showed significant differences between DN and control groups (all $P < 0.05$, **Figure 6D**). Compared to the control group, expression levels of CCL5, IL10RA, RRM2, and THBS2 were upregulated in the DN group, while FGF9 and MAGI2 expressions were downregulated.

Association of six key target genes with T cell function

Given the critical role of T cells in DN, we further explored the association between six key target genes and T cell functional states. As shown in **Figure 7**, THBS2, IL10RA, and CCL5 exhibited significant positive correlations with most T cell states, especially quiescence and regulatory function, which showed strong associations. Conversely, RRM2, MAGI2, and FGF9 were negatively correlated with T cell status. For example, RRM2 displayed a strong negative correlation with cytotoxicity.

Molecular docking revealed high affinity between celastrol and THBS2, FGF9, and MAGI2 in DN

Molecular docking was performed to evaluate the binding affinity between celastrol and the eight marker genes. Based on docking criteria - binding energy < -5.0 kcal/mol and the presence of hydrogen bonds between receptor and ligand [18], the results met the effective docking threshold, as summarized in **Table 1**. Among the targets, THBS2, FGF9, and MAGI2 exhibited strong affinity with celastrol, with binding energies of -7.684, -7.581, and -7.042 kcal/mol, respectively. According to the 3D docking images (**Figure 8A-F**), celastrol forms hydrogen bonds with GLN-757, LEU-758, and ARG-982 of THBS2, ASN-146 of FGF9, and ARG-84 of MAGI2.

Celastrol improved cell viability and attenuated apoptosis, inflammation, and fibrosis in HG-treated HK-2 cells

To validate the protective effects of celastrol against cytotoxicity, apoptosis, inflammation, and fibrosis, an MTT assay, flow cytometry, ELISA, and immunoblotting were conducted in high glucose (HG)-treated HK-2 cells. Exposure to 50 mM glucose significantly reduced the viability of HK-2 cells ($P < 0.001$, Figure S2A), confirming its suitability for DN model induction. To determine the optimal concentration of celastrol, HG-induced cells were exposed to 20, 50 and 100 nM of celastrol. As shown in Figure S2B, 100 nM celastrol significantly reduced HK-2 cell viability compared to 50 nM and 20 nM. Therefore, 50 nM was selected for

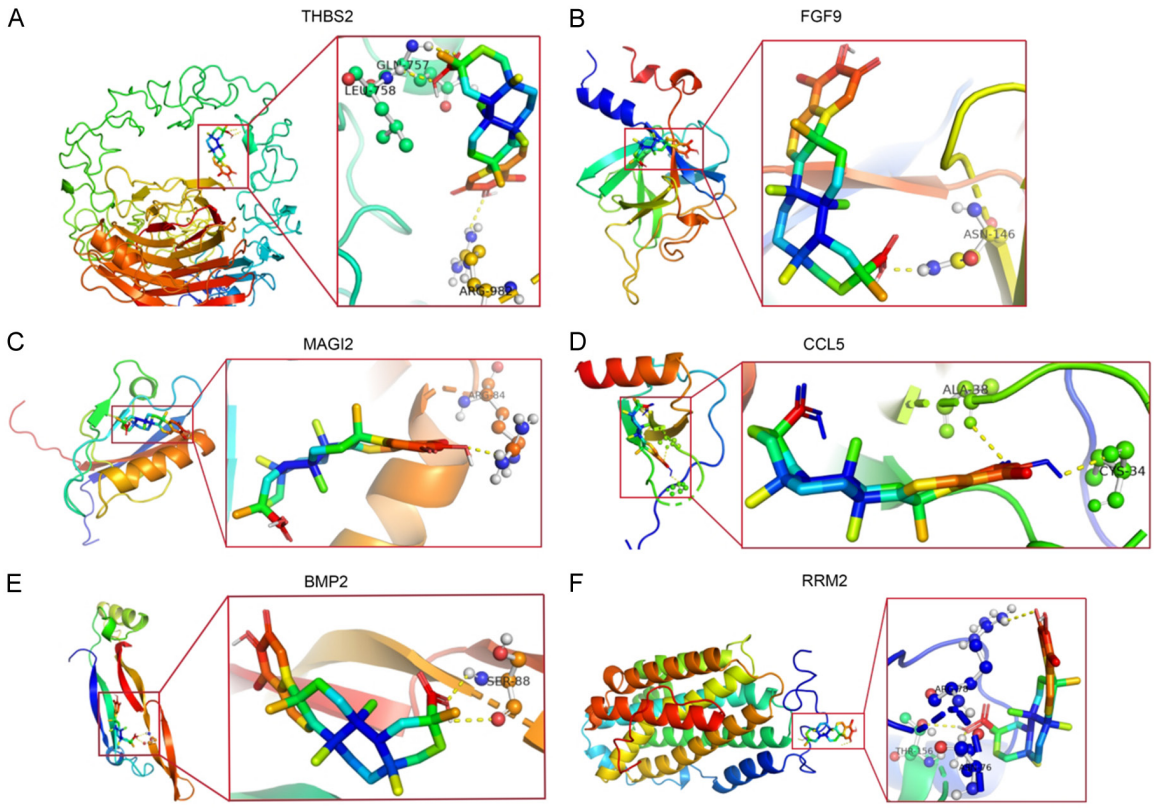

Figure 8. Molecular docking images between celastrol and protein targets. (A-F) Binding form of celastrol with (A) GLN-757, LEU-758, and ARG-982 of THBS2, (B) ASN-146 of FGF9, (C) ARG-84 of MAGI2, (D) ALA-38 and CYS-34 of CCL5, (E) SER-88 of BMP2, and (F) APG-78, THR-156 and ASN-76 of RRM2.

subsequent experiments to minimize potential cytotoxicity. Compared to control cells, HG treatment significantly reduced the HK-2 cell viability and increased apoptosis ($P < 0.001$). Celastrol treatment markedly enhanced cell viability and suppressed apoptosis in HG-induced HK-2 cells ($P < 0.001$, **Figure 9A**, **9B**). Furthermore, celastrol significantly inhibited inflammation and fibrosis in HG-induced HK-2 cells, as evidenced by the reduction in pro-inflammatory cytokines IL-6 and TNF-α, along with decreased expression of fibrosis-related proteins COL-IV, FN, and α-SMA ($P < 0.05$, **Figure 9C**, **9D**). To further validate these findings, western blotting analysis was conducted to assess the expression of the key target proteins identified in the molecular docking (THBS2, MAGI2, and FGF9). In HG-induced cells, THBS2 protein expression was upregulated, while MAFI2 and FGF9 expressions were downregulated. However, celastrol treatment significantly reversed these changes ($P < 0.05$, **Figure 9E**).

Discussion

Diabetic nephropathy (DN) is a leading cause of end-stage renal disease and renal dysfunction, often characterized by tubulointerstitial fibrosis. Celastrol, a bioactive compound known for its anti-inflammatory properties, has been found to prevent the progression of DN [19]. The present study combined bioinformatics analysis and experimental validation to explore the molecular mechanisms through which celastrol exerts its therapeutic effects in DN, particularly by mitigating high glucose-induced damage in HK-2 cells.

The roles of oxidative stress and inflammation in DN are well-established [20]. DN is associated with hypoxia and ROS production, leading to actin cytoskeleton reorganization, cell injury and the development of proteinuria, a sensitive marker for evaluating renal tubule damage [21]. Several pathophysiologic events contribute to the development of DN, including hyperglyce-

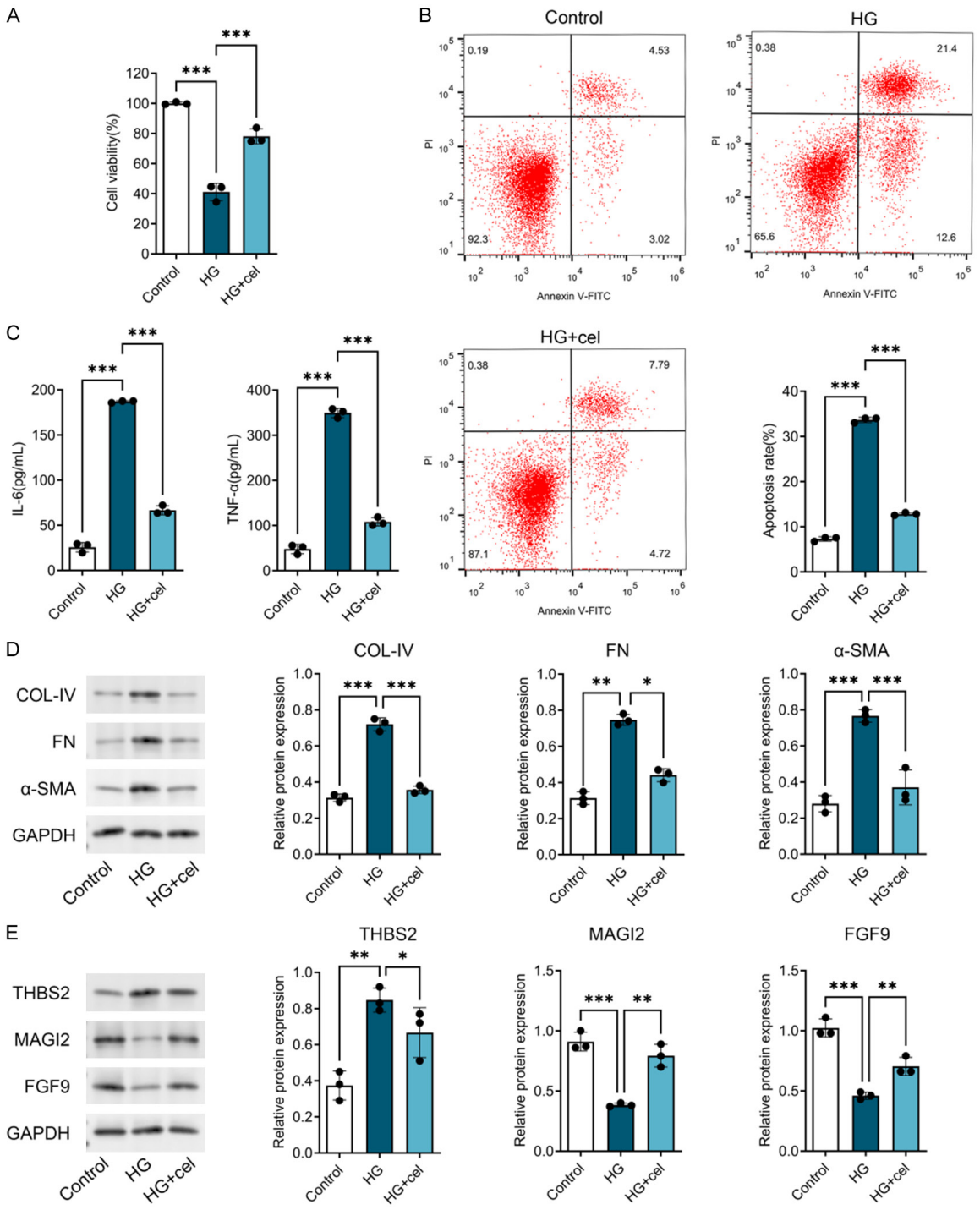

Figure 9. The *in vitro* experiments to validate the protective effects of celastrol against cytotoxicity, apoptosis, inflammation and fibrosis in HG-treated HK-2 cells. A. Cell viability was detected by CCK-8. B. Cell apoptosis was assessed by flow cytometry analysis. C. ELISA was used to determine the levels of IL-6 and TNF-α. D, E. The expression levels of fibrosis-related proteins (COL-IV, FN, and α-SMA) and three key targets (THBS2, MAFI2, and FGF9) were detected using western blotting. Each experiment was performed at least three times; *P < 0.05, **P < 0.01, ***P < 0.001.

mia, hypoxia-induced oxidative stress, and inflammatory responses. The release of ROS triggers the aggregation of inflammatory cells and the formation of inflammatory cytokines, which are crucial in the pathogenesis of DN [22, 23].

Celastrol is widely known for its anti-inflammatory properties. We identified 69 overlapping genes as key targets of celastrol in DN. KEGG enrichment analysis revealed that these targets were involved in multiple signaling pathways, including PI3K-Akt, Rap1, TNF, and MAPK signaling, which are crucial for regulating cellular responses to stress, inflammation, and survival [24-27]. These findings suggest that celastrol exerts multifaceted protective effects against DN. The PI3K/AKT pathway is a key intracellular signaling cascade that regulates various cellular processes, including growth, survival, metabolism, and proliferation [28]. Pathway activity scores analysis through GSVA showed that the PI3K/Akt pathway was significantly upregulated in DN samples compared to controls, consistent with a previous report [29]. In diabetes, hemodynamic changes abnormally activate the PI3K/Akt pathway, inducing cell autophagy and inhibiting their adhesion capacity [30, 31]. Targeting the PI3K/Akt pathway is a promising therapeutic strategy for DN. Previous studies have shown that celastrol can induce autophagy through the PI3K/Akt signaling pathway [32] and ameliorates early-stage DN progression in rats by the PI3K/Akt modulation [33]. Additionally, GSVA also revealed significant activation of the NF-κB signaling pathway and inflammatory pathways in DN. NF-κB pathway is a classic inflammation-related pathway that is often hyperactivated under glucotoxic conditions, ultimately leading to renal injury [34]. Several studies have indicated that some traditional Chinese herbs mitigate DN-related inflammation by regulating PI3K-Akt-mediated NF-κB signaling pathway [35, 36]. In this study, PI3K/Akt pathway scores were significantly correlated with the key celastrol targets, leading us to hypothesize that celastrol may inhibit inflammatory response in DN by regulating the PI3K-Akt/NF-κB pathway.

To further investigate the association between celastrol and inflammation in DN, immune infiltration analysis was performed, given the pivotal role of immune cells in the inflammatory response. Our analysis highlighted significant differences in CD4 and CD8 T cell infiltration between DN and control groups. Elevated T cells in the kidney contribute to chronic inflammation, a given the pivotal role of DN progression [37, 38]. Furthermore, T cell state scores, including terminal exhaustion, senescence, quiescence, cytotoxicity, helper function, and regulatory activity, were higher in DN samples compared to controls. These findings suggest that chronic inflammatory microenvironment in DN may induce persistent T cell activation, enhancing their cytotoxic and helper functions. However, this prolonged stimulation may also lead to T cell depletion and senescence, resulting in an imbalanced immune response. CD8 T cells are primarily associated with cytotoxic activity. A previous study demonstrated that inhibiting CD8 T cell responses alleviates DN in rats [39]. In the present study, celastrol significantly reduced IL-6 and TNF-α levels in HG-induced HK-2 cells. Consistent with previous studies, DN patients have elevated pro-inflammatory cytokines, including IL-1β, IL-6, and TNF-α, reinforcing the importance of anti-inflammatory therapy in DN management [40]. These results suggest that celastrol may modulate the immune response in DN by modulating T cell activity and suppressing inflammatory cytokines, thereby altering the inflammatory microenvironment in DN.

We developed a diagnostic model, comprising eight marker genes (THBS2, MAGI2, FGF9, NLRP3, IL10RA, BMP2, RRM2, and CCL5) that showed excellent diagnostic performance in distinguishing DN from control samples. The high values of AUC in both the training and external validation datasets underscore the robustness and potential clinical utility of this model. Additionally, the eight targets were significantly associated with the T cell states. Molecular docking analysis showed that THBS2, MAGI2, and FGF9 exhibited strong binding affinities with celastrol, suggesting that these genes play key roles in the therapeutic properties of celastrol against DN. THBS2 is involved in apoptosis, cell adhesion, and tissue fibrosis [41, 42], and its expression is significantly elevated in type 2 diabetes patients with nephropathy [43]. FGF9 is also associated with fibrosis, and a bioinformatics study identified it as a gene associated with DN [17]. In HG-treated podocytes, FGF9 expression was significantly reduced [44]. MAGI2 is closely related to the development of nephropathy, interacting with nephrin and regulating the cell cytoskeleton [45, 46]. MAGI2 knockout induced cell dysfunction in DN mice [47]. Consistent with previous studies, we observed that THBS2 expression was upregulated, while MAGI2 and FGF9 were downregulated in HG-induced HK-2 cells. Molecular docking results suggested that celastrol might directly interact with these proteins, forming hydrogen bonds with key residues. In

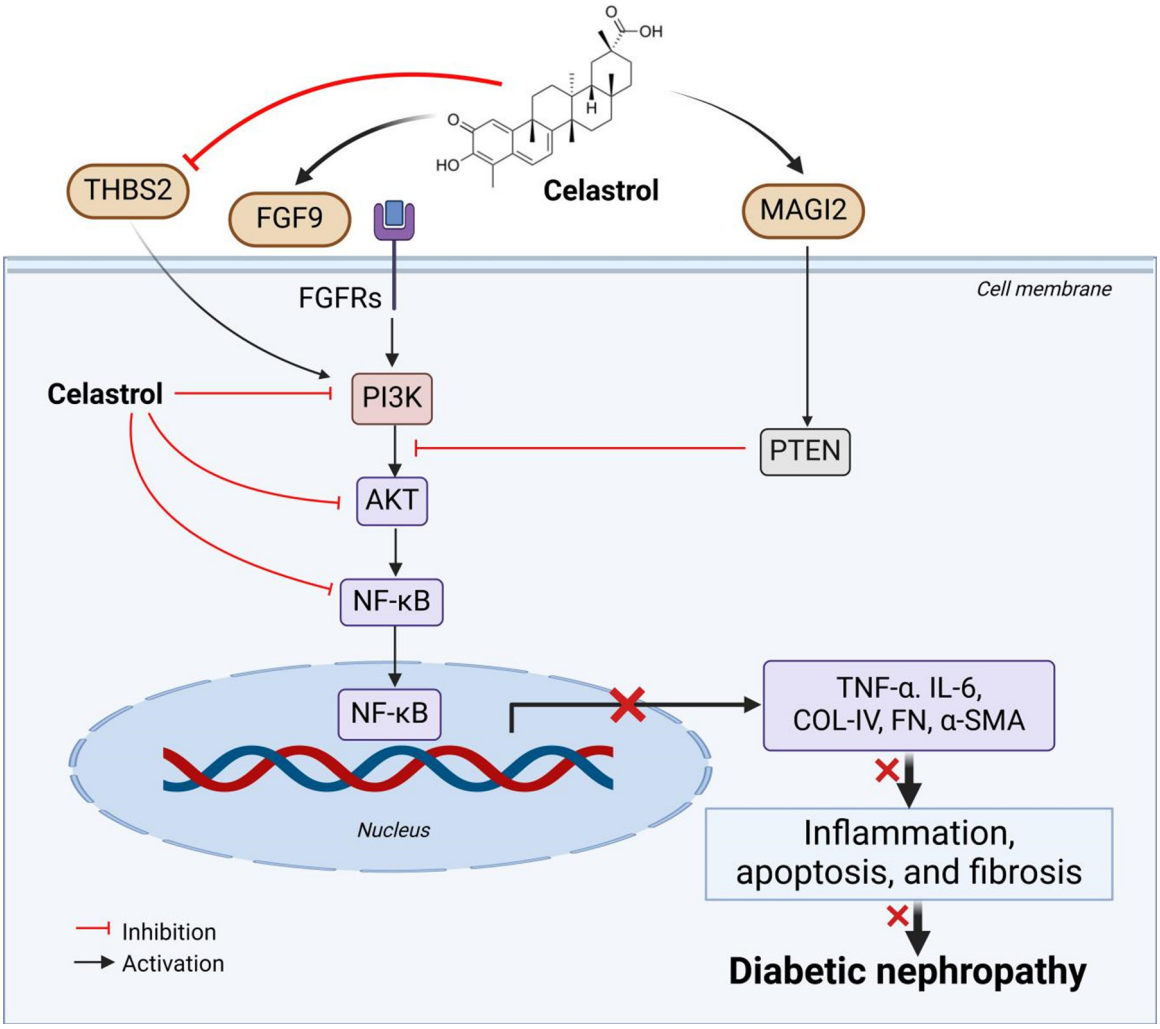

Figure 10. Proposed mechanistic targets of celastrol in alleviating DN and mitigating glucotoxicity-induced HK-2 cells. In the event of high glucose, celastrol exerts its effects by inhibiting THBS2 and upregulating FGF9 and MAGI2, thereby inhibiting the PI3K/Akt pathway. These actions result in decreased NF-κB activity, leading to reduced expression of inflammatory and fibrotic markers such as TNF-α, IL-6, COL-IV, FN, and α-SMA. This combination of effects ultimately suppresses inflammation, apoptosis, and fibrosis, thereby ameliorating DN. DN, diabetic nephropathy.

subsequent validation experiments, celastrol effectively reversed the HG-induced changes in the expression of these proteins, supporting its role in modulating these targets to exert therapeutic effects on DN.

In addition, research has indicated that these three target genes are also associated with the PI3K/Akt signaling pathway. The regulation of PI3K/Akt signaling by THBS2 has been validated in various diseases [48]. For instance, Mo et al. discovered that miR-1228 suppressed PI3K/Akt signaling pathway activation in HG-induced HK-2 cells by targeting THBS2 [49]. FGF9 activates the receptor tyrosine kinase FGFR2 through the PI3K/Akt signaling pathway to inhibit cardiomyocyte apoptosis [50]. MAGI2 downregulates PD-L1 by inhibiting the PI3K/Akt signaling pathway, thereby modulating immune evasion in breast cancer [51]. Notably, in this study, MAGI2 proved to be inversely related to T cell cytotoxicity and helper function, highlighting its likely role in CD4 and CD8 T cells. Conversely, THBS2 showed a positive correlation with T cell regulation and senescence, while FGF9 showed a negative association with T cell regulation and senescence. These results suggest that celastrol may regulate the PI3K/Akt pathway through these key targets, influencing the immune microenvironment and thereby inhibiting the progression of DN (**Figure 10**).

Despite these findings, our study has certain limitations. The conclusions were primarily based on bioinformatics analyses and *in vitro* validations. Further experimental studies are essential to fully elucidate the precise mechanisms by which celastrol mitigates inflammation, apoptosis, and fibrosis in kidney cells under a glucotoxicity environment. These studies are vital to understanding how celastrol alleviates the progression of DN. Importantly, integrated multi-omics analyses are needed to validate the regulatory interactions between celastrol and its key protein targets, including THBS2, MAGI2, and FGF9. These analyses will help uncover the underlying mechanisms of celastrol's therapeutic effects and clarify its potential as a multi-targeted treatment for DN-related disorders.

Conclusion

The study demonstrates that celastrol plays a multifaceted role in mitigating DN by targeting key genes and proteins involved in oxidative stress, inflammation, and immune responses, with a particular emphasis on the PI3K/Akt signaling pathway. The modulation of key genes such as THBS2, FGF9, and MAGI2 highlights their critical involvement in the pathogenesis of DN and their use as therapeutic targets for celastrol. Overall, these findings suggest that celastrol holds significant promise as a therapeutic agent for DN, by targeting multiple pathways to attenuate inflammation, fibrosis, and metabolic dysfunction.

Acknowledgements

This work was supported by the Research University (Individual) Grant Universiti Sains Malaysia (Ref No.: 1001/PTEKIND/8011116) and Shandong Province Traditional Chinese Medicine Science and Technology Project (Ref No.: M-2023158).

Disclosure of conflict of interest

None.

Address correspondence to: Dr. Mohamad Hafizi Abu Bakar, Bioprocess Technology Division, School of Industrial Technology, Universiti Sains Malaysia, Gelugor 11800, Penang, Malaysia. Tel: +604-6535213; E-mail: mhafizi88@usm.my

References

[1] Cui W, Min X, Xu X, Du B and Luo P. Role of nuclear factor erythroid 2-related factor 2 in diabetic nephropathy. J Diabetes Res 2017; 2017: 3797802.

[2] Pelle MC, Provenzano M, Busutti M, Porcu CV, Zaffina I, Stanga L and Arturi F. Up-date on diabetic nephropathy. Life (Basel) 2022; 12: 1202.

[3] Strutz FM. EMT and proteinuria as progression factors. Kidney Int 2009; 75: 475-481.

[4] Su J, Peng J, Wang L, Xie H, Zhou Y, Chen H, Shi Y, Guo Y, Zheng Y, Guo Y, Dong Z, Zhang X and Liu H. Identification of endoplasmic reticulum stress-related biomarkers of diabetes nephropathy based on bioinformatics and machine learning. Front Endocrinol (Lausanne) 2023; 14: 1206154.

[5] Collins AJ, Foley RN, Chavers B, Gilbertson D, Herzog C, Johansen K, Kasiske B, Kutner N, Liu J, St Peter W, Guo H, Gustafson S, Heubner B, Lamb K, Li S, Li S, Peng Y, Qiu Y, Roberts T, Skeans M, Snyder J, Solid C, Thompson B, Wang C, Weinhandl E, Zaun D, Arko C, Chen SC, Daniels F, Ebben J, Frazier E, Hanzlik C, Johnson R, Sheets D, Wang X, Forrest B, Constantini E, Everson S, Eggers P and Agodoa L. United States renal data system 2011 annual data report: atlas of chronic kidney disease & end-stage renal disease in the United States. Am J Kidney Dis 2012; 59 Suppl 1: A7, e1-420.

[6] Chen Y, Lee K, Ni Z and He JC. Diabetic kidney disease: challenges, advances, and opportunities. Kidney Dis (Basel) 2020; 6: 215-225.

[7] Hu Q, Jiang L, Yan Q, Zeng J, Ma X and Zhao Y. A natural products solution to diabetic nephropathy therapy. Pharmacol Ther 2023; 241: 108314.

[8] Elendu C, John Okah M, Fiemotongha KDJ, Adeyemo BI, Bassey BN, Omeludike EK and Obidigbo B. Comprehensive advancements in the prevention and treatment of diabetic nephropathy: a narrative review. Medicine (Baltimore) 2023; 102: e35397.

[9] Luo P, Liu D, Zhang Q, Yang F, Wong YK, Xia F, Zhang J, Chen J, Tian Y, Yang C, Dai L, Shen HM and Wang J. Celastrol induces ferroptosis in activated HSCs to ameliorate hepatic fibrosis via targeting peroxiredoxins and HO-1. Acta Pharm Sin B 2022; 12: 2300-2314.

[10] Xu H, Zhao H, Ding C, Jiang D, Zhao Z, Li Y, Ding X, Gao J, Zhou H, Luo C, Chen G, Zhang A, Xu YZ and hang H. Celastrol suppresses colorectal cancer via covalent targeting peroxiredoxin 1. Signal Transduct Target Ther 2023; 8: 51.

[11] Luo P, Zhang Q, Zhong TY, Chen JY, Zhang JZ, Tian Y, Zheng LH, Yang F, Dai LY, Zou C, Li ZJ,

Liu JH and Wang JG. Celastrol mitigates inflammation in sepsis by inhibiting the PKM2-dependent Warburg effect. Mil Med Res 2022; 9: 22.
[12] Abu Bakar MH, Nor Shahril NS, Mohamad Khalid MSF, Mohammad S, Shariff KA, Karunakaran T, Mohd Salleh R and Mohamad Rosdi MN. Celastrol alleviates high-fat diet-induced obesity via enhanced muscle glucose utilization and mitochondrial oxidative metabolism-mediated upregulation of pyruvate dehydrogenase complex. Toxicol Appl Pharmacol 2022; 449: 116099.
[13] Li X Sr, Liu W, Jiang G, Lian J, Zhong Y, Zhou J, Li H, Xu X, Liu Y, Cao C, Tao J, Cheng J, Zhang JH and Chen G. Celastrol ameliorates neuronal mitochondrial dysfunction induced by intracerebral hemorrhage via targeting cAMP-activated exchange protein-1. Adv Sci (Weinh) 2024; 11: e2307556.
[14] Gu J, Shi YN, Zhu N, Li HF, Zhang CJ and Qin L. Celastrol functions as an emerging manager of lipid metabolism: mechanism and therapeutic potential. Biomed Pharmacother 2023; 164: 114981.
[15] Tang Y, Wan F, Tang X, Lin Y, Zhang H, Cao J and Yang R. Celastrol attenuates diabetic nephropathy by upregulating SIRT1-mediated inhibition of EZH2related wnt/β-catenin signaling. Int Immunopharmacol 2023; 122: 110584.
[16] Tang YL, Dong XY, Zeng ZG and Feng Z. Gene expression-based analysis identified NTNG1 and HGF as biomarkers for diabetic kidney disease. Medicine (Baltimore) 2020; 99: e18596.
[17] Li Z, Liu J, Wang W, Zhao Y, Yang D and Geng X. Investigation of hub genes involved in diabetic nephropathy using biological informatics methods. Ann Transl Med 2020; 8: 1087.
[18] Feng C, Zhao M, Jiang L, Hu Z and Fan X. Mechanism of modified danggui sini decoction for knee osteoarthritis based on network pharmacology and molecular docking. Evid Based Complement Alternat Med 2021; 2021: 6680637.
[19] Zhan X, Yan C, Chen Y, Wei X, Xiao J, Deng L, Yang Y, Qiu P and Chen Q. Celastrol antagonizes high glucose-evoked podocyte injury, inflammation and insulin resistance by restoring the HO-1-mediated autophagy pathway. Mol Immunol 2018; 104: 61-68.
[20] Jin Q, Liu T, Qiao Y, Liu D, Yang L, Mao H, Ma F, Wang Y, Peng L and Zhan Y. Oxidative stress and inflammation in diabetic nephropathy: role of polyphenols. Front Immunol 2023; 14: 1185317.
[21] Kang JS, Lee SJ, Lee JH, Kim JH, Son SS, Cha SK, Lee ES, Chung CH and Lee EY. Angiotensin II-mediated MYH9 downregulation causes structural and functional podocyte injury in diabetic kidney disease. Sci Rep 2019; 9: 7679.
[22] Konishi M, Shindo N, Komiya M, Tanaka K, Itoh T and Hirota T. Quantitative analyses of the metaphase-to-anaphase transition reveal differential kinetic regulation for securin and cyclin B1. Biomed Res 2018; 39: 75-85.
[23] Qiu Y, Tang J, Zhao Q, Jiang Y, Liu YN and Liu WJ. From diabetic nephropathy to end-stage renal disease: the effect of chemokines on the immune system. J Diabetes Res 2023; 2023: 3931043.
[24] Lei L, Zhao J, Liu XQ, Chen J, Qi XM, Xia LL and Wu YG. Wogonin alleviates kidney tubular epithelial injury in diabetic nephropathy by inhibiting PI3K/Akt/NF-κB signaling pathways. Drug Des Devel Ther 2021; 15: 3131-3150.
[25] Li B, Zhao X, Xie W, Hong Z and Zhang Y. Integrative analyses of biomarkers and pathways for diabetic nephropathy. Front Genet 202; 14: 1128136.
[26] Navarro JF and Mora-Fernández C. The role of TNF-alpha in diabetic nephropathy: pathogenic and therapeutic implications. Cytokine Growth Factor Rev 2006; 17: 441-450.
[27] Gong P, Wang P, Pi S, Guo Y, Pei S, Yang W, Chang X, Wang L and Chen F. Proanthocyanidins protect against cadmium-induced diabetic nephropathy through p38 MAPK and Keap1/Nrf2 signaling pathways. Front Pharmacol 2021; 12: 801048.
[28] Tang G, Du Y, Guan H, Jia J, Zhu N, Shi Y, Rong S and Yuan W. Butyrate ameliorates skeletal muscle atrophy in diabetic nephropathy by enhancing gut barrier function and FFA2-mediated PI3K/Akt/mTOR signals. Br J Pharmacol 2022; 179: 159-178.
[29] Wu W, Hu W, Han WB, Liu YL, Tu Y, Yang HM, Fang QJ, Zhou MY, Wan ZY, Tang RM, Tang HT and Wan YG. Inhibition of Akt/mTOR/p70S6K signaling activity with huangkui capsule alleviates the early glomerular pathological changes in diabetic nephropathy. Front Pharmacol 2018; 9: 443.
[30] Takeuchi H, Kondo Y, Fujiwara K, Kanzawa T, Aoki H, Mills GB and Kondo S. Synergistic augmentation of rapamycin-induced autophagy in malignant glioma cells by phosphatidylinositol 3-kinase/protein kinase B inhibitors. Cancer Res 2005; 65: 3336-3346.
[31] Ou Y, Zhang W, Chen S and Deng H. Baicalin improves podocyte injury in rats with diabetic nephropathy by inhibiting PI3K/Akt/mTOR signaling pathway. Open Med (Wars) 2021; 16: 1286-1298.
[32] Yang J, Liu J, Li J, Jing M, Zhang L, Sun M, Wang Q, Sun H, Hou G, Wang C and Xin W. Celastrol inhibits rheumatoid arthritis by inducing autophagy via inhibition of the PI3K/AKT/mTOR signaling pathway. Int Immunopharmacol 2022; 112: 109241.

[33] Nie Y, Fu C, Zhang H, Zhang M, Xie H, Tong X, Li Y, Hou Z, Fan X and Yan M. Celastrol slows the progression of early diabetic nephropathy in rats via the PI3K/AKT pathway. BMC Complement Med Ther 2020; 20: 321.
[34] Ma X, Ma J, Leng T, Yuan Z, Hu T, Liu Q and Shen T. Advances in oxidative stress in pathogenesis of diabetic kidney disease and efficacy of TCM intervention. Ren Fail 2023; 45: 2146512.
[35] Hong JN, Li WW, Wang LL, Guo H, Jiang Y, Gao YJ, Tu PF and Wang XM. Jiangtang decoction ameliorate diabetic nephropathy through the regulation of PI3K/Akt-mediated NF-κB pathways in KK-Ay mice. Chin Med 2017; 12: 13.
[36] Meng X, Ma J, Kang SY, Jung HW and Park YK. Jowiseungki decoction affects diabetic nephropathy in mice through renal injury inhibition as evidenced by network pharmacology and gut microbiota analyses. Chin Med 2020; 15: 24.
[37] CNavarro-González JF and Mora-Fernández C. The role of inflammatory cytokines in diabetic nephropathy. J Am Soc Nephrol 2008; 19: 433-442.
[38] Chen J, Liu Q, He J and Li Y. Immune responses in diabetic nephropathy: pathogenic mechanisms and therapeutic target. Front Immunol 2022; 13: 958790.
[39] Zhang F, Wang C, Wen X, Chen Y, Mao R, Cui D, Li L, Liu J, Chen Y, Cheng J and Lu Y. Mesenchymal stem cells alleviate rat diabetic nephropathy by suppressing CD103(+) DCs-mediated CD8(+) T cell responses. J Cell Mol Med 2020; 24: 5817-5831.
[40] Zhang T, Sun W, Wang L, Zhang H, Wang Y, Pan B, Li H, Ma Z, Xu K, Cui H and Lv S. Rosa laevigata Michx. Polysaccharide ameliorates diabetic nephropathy in mice through inhibiting ferroptosis and PI3K/AKT pathway-mediated apoptosis and modulating tryptophan metabolism. J Diabetes Res 2023; 2023: 9164883.
[41] Zhang S, Yang H, Xiang X, Liu L, Huang H and Tang G. THBS2 is closely related to the poor prognosis and immune cell infiltration of gastric cancer. Front Genet 2022; 13: 803460.
[42] Hsu CH, Liu IF, Kuo HF, Li CY, Lian WS, Chang CY, Chen YH, Liu WL, Lu CY, Liu YR, Lin TC, Lee TY, Huang CY, Hsieh CC and Liu PL. miR-29a-3p/THBS2 axis regulates PAH-induced cardiac fibrosis. Int J Mol Sci 2021; 22: 10574.
[43] Yeh SH, Chang WC, Chuang H, Huang HC, Liu RT and Yang KD. Differentiation of type 2 diabetes mellitus with different complications by proteomic analysis of plasma low abundance proteins. J Diabetes Metab Disord 2015; 15: 24.
[44] Chen S, Li B, Chen L and Jiang H. Identification and validation of immune-related biomarkers and potential regulators and therapeutic targets for diabetic kidney disease. BMC Med Genomics 2023; 16: 90.
[45] Zhang H, Lin L, Liu J, Pan L, Lin Z, Zhang M, Zhang J, Cao Y, Zhu J and Zhang R. Phase separation of MAGI2-mediated complex underlies formation of slit diaphragm complex in glomerular filtration barrier. J Am Soc Nephrol 2021; 32: 1946-1960.
[46] Bierzynska A, Soderquest K, Dean P, Colby E, Rollason R, Jones C, Inward CD, McCarthy HJ, Simpson MA, Lord GM, Williams M, Welsh GI, Koziell AB and Saleem MA; NephroS; UK study of Nephrotic Syndrome. MAGI2 mutations cause congenital nephrotic syndrome. J Am Soc Nephrol 2017; 28: 1614-1621.
[47] Zhu B, Cao A, Li J, Young J, Wong J, Ashraf S, Bierzynska A, Menon MC, Hou S, Sawyers C, Campbell KN, Saleem MA, He JC, Hildebrandt F, D'Agati VD, Peng W and Kaufman L. Disruption of MAGI2-RapGEF2-Rap1 signaling contributes to podocyte dysfunction in congenital nephrotic syndrome caused by mutations in MAGI2. Kidney Int 2019; 96: 642-655.
[48] Xu P, Feng DX, Wang J, Wang YD, Xie G, Zhang B, Li XH, Zeng JW and Feng JF. LncRNA AGAP2 antisense RNA 1 stabilized by insulin-like growth factor 2 mRNA binding protein 3 promotes macrophage M2 polarization in clear cell renal cell carcinoma through regulation of the microRNA-9-5p/THBS2/PI3K-Akt pathway. Cancer Cell Int 2023; 23: 330.
[49] Mo T, Fu Q, Hu X, Fu Y and Li J. MicroRNA 1228 mediates the viability of high glucose-cultured renal tubule cells through targeting thrombospondin 2 and PI3K/AKT signaling pathway. Kidney Blood Press Res 2022; 47: 1-12.
[50] Shi HJ, Wang MW, Sun JT, Wang H, Li YF, Chen BR, Fan Y, Wang SB, Wang ZM, Wang QM and Wang LS. A novel long noncoding RNA FAF inhibits apoptosis via upregulating FGF9 through PI3K/AKT signaling pathway in ischemia-hypoxia cardiomyocytes. J Cell Physiol 2019; 234: 21973-21987.
[51] Yao X, Tu Y, Xu Y, Guo Y, Yao F and Zhang X. Endoplasmic reticulum stress-induced exosomal miR-27a-3p promotes immune escape in breast cancer via regulating PD-L1 expression in macrophages. J Cell Mol Med 2020; 24: 9560-9573.

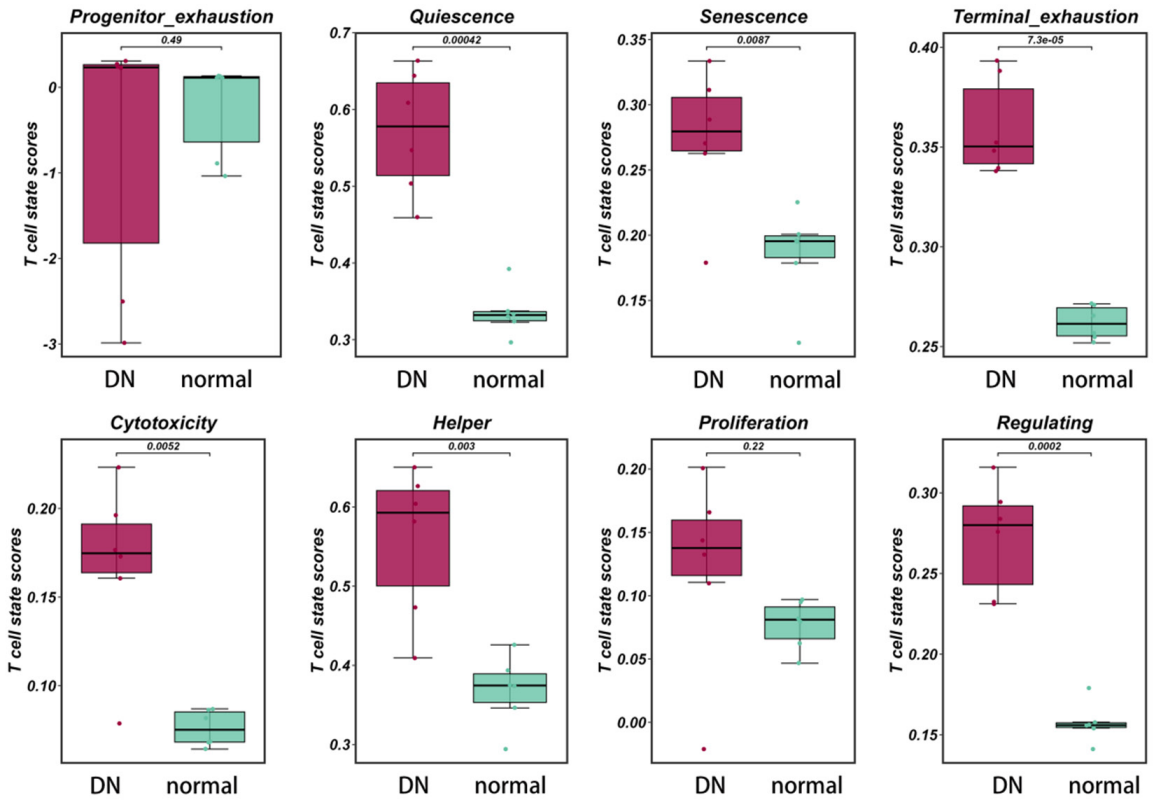

Figure S1. Eight state scores of T cells in DN and normal samples. DN, diabetic nephropathy.

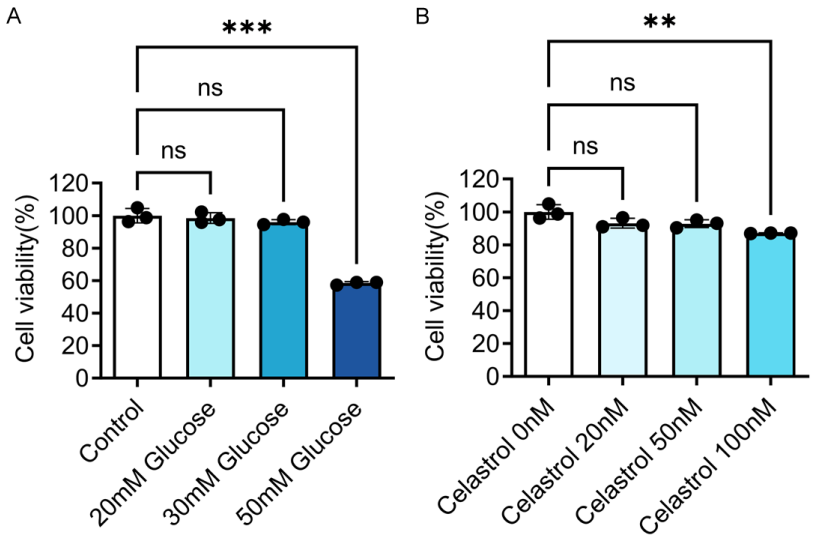

Figure S2. Cell viability of HK-2 cells treated with glucose and celastrol. A. The cells were exposed to three different concentrations (20, 30 and 50 mM) of glucose. B. The high glucose-treated cells were subsequently incubated with celastrol at three different concentrations (20, 50 and 100 nM). NS: not significant, **P < 0.01, ***P < 0.001.